Submission to: *Journal of Cell Biology*

$VEGF_{165}$ Stimulates Vessel Density and Vessel Diameter Differently in Angiogenesis and Lymphangiogenesis

Patricia Parsons-Wingerter,[1,3] Krishnan Radhakrishnan,[2] Paul E. DiCorleto,[3] Dmitry Leontiev,[4] Bela Anand-Apte,[5] Brian Albarran,[6] Andrew G. Farr[7]

[1]Biological Fluid Physics and [2]ICOMP, NASA Glenn Research Center, Cleveland, OH 44135

[3]Department of Cell Biology and [4]Imaging Core Facility, The Lerner Research Institute and [5]Cole Eye Institute, Cleveland Clinic Foundation, Cleveland, OH 44195

Departments of [6]Biomedical Engineering and [7]Biological Structure, University of Washington School of Medicine, Seattle, WA 98195

Address correspondence to:
Patricia Parsons-Wingerter, Ph.D.
Biological Fluid Physics
NASA Glenn Research Center
B110-3
Cleveland, OH 44135

Tel. 1-216-433-8796, Fax 1-216-433-3793
E-mail: patricia.parsons@grc.nasa.gov

Number of characters: 47,509
Running Title: VEGF Stimulation of Vascular and Lymphatic Vessels

ABSTRACT

Vascular endothelial growth factor-165 ($VEGF_{165}$) stimulated angiogenesis in the quail chorioallantoic membrane (CAM) by vessel expansion from the capillary network. However, lymphangiogenesis was stimulated by the filopodial guidance of tip cells located on blind-ended lymphatic sprouts. As quantified by fractal/generational branching analysis using the computer code VESGEN, vascular density increased maximally at low VEGF concentrations, and vascular diameter increased most at high VEGF concentrations. Increased vascular density and diameter were statistically independent events (r_s, -0.06). By fluorescence immunohistochemistry of VEGF receptors VEGFR-1 and VEGFR-2, alpha smooth muscle actin (αSMA) and a vascular/lymphatic marker, $VEGF_{165}$ increased the density and diameter of sprouting lymphatic vessels guided by tip cells (accompanied by the dissociation of lymphatics from blood vessels). Isolated migratory cells expressing αSMA were recruited to blood vessels, whereas isolated cells expressing VEGFR-2 were recruited primarily to lymphatics. In conclusion, $VEGF_{165}$ increased lymphatic vessel density by lymphatic sprouting, but increased blood vessel density by vascular expansion from the capillary network.

Key Words: angiogenesis; lymphangiogenesis; vascular endothelial growth factor; VEGF; fractal; vascular; lymphatic; filopodia; chorioallantoic membrane; CAM; quail; avian.

INTRODUCTION

We must understand all modes of angiogenesis and lymphangiogenesis for effective therapeutic targeting of pathological vascular and lymphatic remodeling. Developmental models are useful for initial identification and understanding of the several modes of vessel formation and growth. For example, in the early mouse allantois and quail dorsal aorta, the first blood vessels form as vascular networks by the process termed vasculogenesis (Argraves et al., 2002; Risau and Flamme, 1995). In the postnatal mouse retina, the initial vascular network (plexus) is expanded by sprouting vessels guided by the filopodia of endothelial tip cells (Gerhardt et al., 2003), and the homogeneous network is pruned into a more mature vascular tree by cells expressing αSMA (Benjamin et al., 1998). We report that angiogenesis in the maturing quail chorioallantoic membrane (CAM) differs from the other developmental modes of angiogenesis and vasculogenesis described above. In the mid-stage developing CAM, vascular endothelial growth factor-165 ($VEGF_{165}$) increases the growth of new blood vessels by vascular expansion from the pre-existing capillary network. Lymphangiogenesis is stimulated, however, by the filopodial guidance of tip cells located at the ends of sprouting lymphatic vessels (Gerhardt et al., 2003).

$VEGF_{165}$, generally the most angiogenic isoform of VEGF-A, is an endothelial-specific mitogen, chemoattractant, permeability agent and vascular maturational factor (Ferrara et al., 2003; Nagy et al., 2003). The VEGF family currently comprises five members, VEGF-A through -E. Effects of the VEGF's on vascular morphology are not highly quantified because of the complex, three-dimensional (3D) spatial patterns of

most branching vascular and lymphatic trees. Increased VEGF expression during angiogenesis and lymphangiogenesis is well-established (Ferrara et al., 2003; Neufeld et al., 1999), but the pleomorphic activities of VEGF's *in vivo* are complex and sometimes contradictory.

We previously described a model of angiogenesis *in vivo* in which the 2D vasculature of the transparent, rapidly developing quail CAM is easily and uniformly exposed to angiogenic stimulators or inhibitors in solution (Parsons et al., 1998; 2000a; 2000b). Spatial patterns of the branching vascular tree and associated capillary network are visualized by light and fluorescence microscopy, and then quantified by fractal-based branching analysis. Each regulator of angiogenesis tested previously in the CAM, including basic fibroblast growth factor (bFGF or FGF-2), transforming growth factor-β1 (TGF-β1) and angiostatin, elicited a simple, robust, unimodal vascular pattern that was spatiotemporally unique and characterized by strong statistical confidence (i.e., low sample variation).

In contrast, vascular and lymphatic response to $VEGF_{165}$ in the quail CAM was complex and multimodal. $VEGF_{165}$ increased both the density and diameter of vascular and lymphatic vessels. Increased vascular diameter was associated with increased vascular leakage, and smaller blood vessels frequently became more tortuous. By fractal-based branching analysis, increases in vascular density and diameter were measured as independent but overlapping effects of increasing $VEGF_{165}$ concentration that reached maximal frequencies at low and high cytokine concentration, respectively. $VEGF_{165}$ selectively stimulated the growth of new, small vessels, as quantified by

VESGEN, a computerized generational analysis of vascular branching. Fluorescent immunohistochemistry (IHC) of the VEGF receptors VEGFR-1 (flt-1) and VEGFR-2 (KDR/flk-1), alpha smooth muscle actin (αSMA) and the QH-1 vascular marker revealed that that $VEGF_{165}$ (1) increased the frequency of vascular and lymphatic anastomoses, (2) increased the diameter and density of lymphatic vessels and (3) induced the anti-maturational, regressive dissociation of lymphatic vessels from blood vessels. Angiogenesis proceeded by the expansion of arterioles and post-capillary venules from the pre-existing capillary bed and the recruitment of numerous, migratory cells expressing αSMA. Lymphangiogenesis was guided by the filopodia of tip cells leading the lymphatic sprouts. Lymphatic tip cells appeared to be derived from a large population of isolated cells expressing VEGFR-2; some of the isolated VEGFR-2+ cells may also have merged with growing blood vessels. Regulation by $VEGF_{165}$ resulted in complex, multimodal vascular change, compared to strong stimulation and inhibition of vascular density as the sole, unimodal response of CAM vessels to bFGF and TGF-β1 (Parsons et al., 2000a; 2000b).

RESULTS

Fractal/VESGEN Analysis of Increased Arterial Density and Diameter

$VEGF_{165}$ stimulated complex, multimodal change during angiogenesis in the CAM when applied at E7 for 24 h, as indicated by binary (black/white) and skeletonized images of arterial endpoints in the vascular tree (Fig. 1). Increased arterial density and diameter were measured by several confirming parameters that include the fractal dimension (D_f), vessel area density (A_V), vessel length density (L_V) and vessel diameter (D_V). Fractal analysis, a recently invented mathematical tool (Mandelbrot, 1983), is useful for the quantification of complex spatial patterns such as branching vascular trees. In 2D binary (black/white) images, D_f is limited by the Euclidean dimensions of 1 and 2. D_f increases with increasing pattern density, and is sensitive to small, early-stage, reproducible changes in the vascular tree (Avakian et al., 2002; Parsons et al., 1998; 2000a; 2000b). Vascular parameters such as A_V, L_V and D_V are measured by the software code VESGEN for CAM branching generations G1 through G≥5 (Fig. 2).

By fractal/VESGEN analysis of skeletonized images, the highest frequencies of increased vessel density were associated with VEGF concentrations of 1.25-2.5 μg/CAM (Fig. 1B, F; Fig. 3A-B). We have found that skeletonized images are sensitive indicators of vessel density (Avakian et al., 2002; Parsons et al., 1998). The highest frequencies of increased vessel diameter in binary images occurred at concentrations of 2.5-5 μg/CAM (Fig. 1C, G; Fig. 3A, C). The two morphological effects of VEGF stimulation were measured independently in separate specimens or in combination (in

the same specimen; Fig. 1D, H), and did not appear to be normally distributed (Fig. 3). We therefore report the standard deviation (SD) only for the control group (0 μg/CAM). Specimens were classified as responders or non-responders to VEGF if the fractal dimension (D_f) or vessel diameter (D_{v1-3}) was greater than or equal to (mean + SD) of the control group.

Stimulation of arterial density by $VEGF_{165}$ reached maximal frequency at 1.25 μg/CAM (six responders out of nine specimens, Fig. 3B; the trend was confirmed by L_v, Table 1). By vessel number density (N_v), increased arterial density in responding groups resulted from growth of new small vessels of $G_{\geq 5}$. Stimulation of vessel diameter measured by D_{v1-3} increased continuously with increasing concentration of $VEGF_{165}$ and was greatest at 2.5-5 μg/CAM (Fig. 3C; seven and six responders out of 10 and 9 specimens, respectively). Although only arterial diameters were quantified, venous diameters in VEGF-treated specimens increased concurrently with increases in arterial diameter. Arterial frequency distributions for D_{v1-4} were highly similar to D_{v1-3}; $D_{v\geq 5}$ in responder populations did not differ significantly from that of control specimens (results not shown). Results for $D_{v\geq 5}$ may be interesting and significant, or may be due to insufficient precision in measuring the diameters of small vessels.

Statistically significant differences for the five treatment groups for 0-5 μg $VEGF_{165}$/CAM were calculated by ANOVA (Table 1), and confirmed results for the responder analysis reported above. For D_f and L_v in skeletonized images, only the treatment groups of 1.25 and 2.5 μg/CAM differed significantly from the control group of 0 μg/CAM (*p*-values for D_f and L_v, 0.07 and 0.16; not shown in Table 1). For D_{v1-3} in

binary images, only the treatment groups of 2.5 and 5 μg/CAM differed significantly from the control group 0 μg/CAM (*p*-values, 0.02 and 0.009; not shown in Table 1).

Stimulation of arterial density and diameter by $VEGF_{165}$ were statistically independent events (i.e., non-correlated). For the entire responder population extracted from the treatment groups of 1.25, 2.5 and 5 μg/CAM (Table 1), the dependence of L_v on increasing D_{v1-3} was negligible according to Spearman's rank correlation coefficient (r_S was −0.06, where −1, 0 and 1 are absolute values of negative correlation, non-correlation and positive correlation). For the entire population combining all specimens (i.e., responders and non-responders) the dependence of L_v on increasing D_{v1-3} also was not significant (r_S = 0.18).

Overall Arterial Stimulation by $VEGF_{165}$

Increased responder frequency in arterial area measured by D_f and arterial area density A_v was essentially constant in binary images for the three highest treatment groups (Fig. 4 and Table 1). Increased arterial area can result from either increased vessel density and/or increased vessel diameter. For each treatment group in Fig. 4B, A_v appeared normally distributed. By ANOVA, the increased arterial area measured by A_v and D_f in the three highest treatment groups (1.25, 2.5 and 5 μg/CAM) differed significantly from the two lowest treatment groups (0 and 0.5 μg/CAM; *p*-values ≤ 0.002, Table 1). The consistent, significant increase in overall arterial area with increasing concentration of $VEGF_{165}$ was very strong (Fig. 4), despite differing trends for increases in vessel density and diameter (Fig. 3). Results suggest that vascular cells

were allocated differently for growth of new, small blood vessels or for increasing the diameters of pre-existing vessels.

Coordinate Stimulation of Angiogenesis and Lymphangiogenesis

The coordinate effect of $VEGF_{165}$ on angiogenesis and lymphangiogenesis at concentrations highly stimulatory of increased vascular density (1.25 μg/CAM) and increased vascular diameter (5 μg/CAM) was further investigated by fluorescence IHC with antibodies recognizing VEGFR-1, VEGFR-2 and αSMA (Figs. 5-8). The QH-1 monoclonal antibody was used as a well-established marker of quail embryonic vasculature, hematopoietic precursor cells and in our hands, lymphatic vessels positive for VEGFR-2, according to lymphatic morphology described previously (Oh et al., 1997). In the 2D, transparent CAM, vascular/lymphatic trees residing in the inner allantoic layer are conveniently separated from the capillary network located in the outer chorionic layer.

Staining for VEGFR-2 and the QH-1 epitope was highly colocalized (Fig. 5A-B), and the endogenous expression of VEGFR-2 was generally reciprocal to that of VEGFR-1 (Fig. 5B-D). In control specimens at E7 and E8 (beginning and end of treatment by $VEGF_{165}$), VEGFR-2 and the QH-1 epitope were intensely expressed on round or elongate isolated cells and on lymphatic vessels, and at low or moderate levels on blood vessels and capillaries (Fig. 5B). VEGFR-1 was: (1) abundantly expressed at the edges of capillaries (Fig. 5D); (2) present at moderate to low levels on blood vessels (appearing more intense on smaller blood vessels), and (3) very low or absent from

lymphatic vessels and isolated cells (Fig. 5C, D). The rather punctate nature of VEGFR-1 expression on capillaries (and outlining of small blood vessels) was confirmed by two different polyclonal antibodies compared to nonspecific IgG controls. The expression of VEGFR-1 (Fig. 5C-G) and VEGFR-2/QH-1 (Fig. 5, 6, 8) was not significantly altered by treatment with $VEGF_{165}$ at 1.25 and 5 μg/CAM.

Vascular and lymphatic response to stimulation by $VEGF_{165}$ resulted in striking morphological changes, however. Increased lymphatic density at 1.25 and 5 μg $VEGF_{165}$/CAM was associated with the increased diameter of lymphatic vessels and an irregular lymphatic morphology more detached from smaller blood vessels, relative to control specimens (Fig. 6A, C-E). The frequent network-like organization of lymphatics resembled the immature lymphatic morphology observed at E5 - E6 in untreated specimens (Fig. 6B). Enlarged lymphatic diameters induced by VEGF (Fig. 6) resembled the diameters of more mature lymphatics observed in control specimens at E9 – E10 (Fig. 8I).

Increased vascular density, accompanied by increased frequency of vascular anastomoses, was observed primarily at 1.25 μg $VEGF_{165}$/CAM (Fig. 7A, C, D). Vascular anastomoses were relatively frequent in normal specimens at E6 - E7 and infrequent at E8 - E10. Increased vascular diameter was observed most frequently in specimens treated with 5 μg $VEGF_{165}$/CAM (results not shown, because increases in vessel diameter are dependent on branching location in the vascular tree; see Figs. 1 and 3).

Single cells expressing αSMA were prominent in control and VEGF-treated samples at E8 and were often visualized as merging with blood vessels (Fig. 7E-G). The

frequency of αSMA-positive cells displaying a migratory phenotype was variable throughout a specimen. Treatment with $VEGF_{165}$ at 1.25 μg/CAM may have increased the numbers of isolated cells expressing VEGFR-2 and αSMA (Figs. 5-7). In control specimens, isolated cells expressing either VEGFR-2/QH-1 or αSMA, were very numerous at E6 - E7, declined in number by E9, and were infrequent at E10.

$VEGF_{165}$ Stimulates Angiogenesis by Vascular Expansion from the Capillary Network

At E7-E8, normal and VEGF-stimulated angiogenesis in the CAM resulted by vascular expansion (i.e., emergence) of arterioles and post-capillary venules from the capillary network (Figs. 7-8). No vascular tip cells displaying extended filopodia and positive expression of VEGFR-2/QH-1 were observed in control or VEGF-treated specimens during this relatively mature phase of angiogenesis in the CAM. The actual initiation of a new branching vessel is not clear from these results. But clearly, new small vessels were elongating by growth from out of the capillary bed, as revealed by both endothelial and smooth muscle staining. In the quail CAM, vascular development is complete at E10 (Parsons et al., 1998). Blood vessels were identified by staining of vascular and endothelial cells and hematopoietic precursors by VEGFR-2/QH-1, and staining of smooth muscle cells or smooth muscle cell precursors by αSMA (Figs. 7-8). Positive expression for αSMA in capillaries seems unusual and was transient (Fig. 7), being no longer visible at E9 and E10 when angiogenesis is complete in the quail CAM. However, mature vessels at E9-E10 still displayed the same transitional, emergent

morphology from capillary bed to small blood vessels (results not shown) that is evident at E7-E8 in control and VEGF-treated specimens. Transient expression of αSMA on the capillaries probably supports remodeling of the capillary network into small blood vessels (Fig. 7A, B), which also proceeds by recruitment of migrating single cells expressing αSMA (Fig. 7E-G).

$VEGF_{165}$ Stimulates Lymphangiogenesis by Filopodial Guidance of Tip Cells

At E7-E8, lymphangiogenesis in control and VEGF-treated specimens (Fig. 6) proceeded by the sprouting of lymphatic vessels guided by the filopodia of tip cells, identified by positive expression of VEGFR-2/QH-1 (Fig. 8). The tip cells appeared to be recruited primarily from a large population of isolated cells that often displayed prominent filopodia. Tip cells were located (1) within the large, well-developed lymphatic networks tightly enclosing larger blood vessels, (2) at the ends of smaller lymphatics loosely associated with smaller blood vessels, and (3) on isolated lymphatics or lymphatic networks in surrounding CAM tissue. Lymphatic tip cells displaying filopodia were very frequently visible at E6-E7 (Fig. 7A-F, E6 not shown), decreasing in number at E8 in control and VEGF-treated specimens. The tip cells were still present at E9, although overall lymphatic architecture was smoother, thicker and accompanied by decreasing numbers of VEGFR-2+ isolated cells (Fig. 8I). Tip cells apparently play a critical role in the development of well-connected lymphatic

networks. Although clearly recruited from isolated precursor cells, it is not known whether tip cells were also produced by cell division within lymphatic sprouts.

DISCUSSION

$VEGF_{165}$ stimulated complex, multimodal change in the vasculature and lymphatics of the quail CAM, in contrast to unimodal vascular changes induced by bFGF and TGF-β1 that were characterized by low sample variation (i.e., low p-values; Parsons et al., 2000a; 2000b). Treatment with $VEGF_{165}$ increased vessel density, vessel diameter, tortuosity of smaller blood vessels and hence, increasingly abnormal vascular and lymphatic morphology in response to increasing cytokine concentration. Utilizing two different morphological mechanisms, VEGF stimulated angiogenesis by vascular expansion from the capillary bed, whereas lymphangiogenesis proceeded by filopodial guidance of tip cells located on sprouting lymphatic vessels (Fig. 9). During vascular expansion in the VEGF-stimulated and control quail CAM at E7-E8, when the vasculature is maturing but still strongly angiogenic (Parsons et al., 1998), large numbers of isolated cells expressing αSMA were recruited to growing blood vessels (Fig. 7). During lymphangiogenesis at E7 - E9, isolated cells positive for the expression of VEGFR-2 and the QH-1 epitope were recruited as tip cells to the growing lymphatic sprouts (Fig. 8).

Several morphological modes of VEGF-regulated angiogenesis and vasculogenesis have been described previously in the developing mouse and quail. Signaling by VEGF-A was required for proper assembly of the spatially homogeneous vascular network or plexus in the mouse allantois and developing quail aorta (Argraves et al., 2002). In the postnatal mouse retina, the initial endothelial plexus was pruned into a more mature vascular tree by cells expressing αSMA and regulated by PDGF-B and VEGF (Benjamin et al., 1998). The vascular plexus expanded at the periphery by

guidance of filopodial tip cells on sprouting vessels under the regulation of VEGF-A (Gerhardt et al., 2003). The complex regulation of angiogenesis and lymphangiogenesis by the VEGF family is tissue and program-specific (Byzova et al., 2002).

By region-based fractal/VESGEN analysis of the CAM arterial tree, we conclude that increased vascular density and diameter were overlapping but statistically independent and reciprocal responses to increasing VEGF concentration (i.e., decreased arterial density as measured by D_f and L_v was accompanied by increased arterial diameter as measured by D_v). Increased area density in response to VEGF was essentially constant in the three responding treatment groups (A_v and D_f at 1.25, 2.5 and 5 μg $VEGF_{165}$/CAM, Fig. 4 and Table 1). Results for A_v, L_v, D_v and D_f suggest that $VEGF_{165}$ stimulated a constant rate of vascular cell proliferation, but that vascular cells were selectively recruited for contribution to either increased arterial density or diameter.

Increased arterial density in VEGF-treated responder groups resulted from selective stimulation of the growth of new small vessels of $G_{\geq 5}$, as measured by the computer code VESGEN. Regulation by bFGF and TGF-β1 also targeted respectively the stimulation and inhibition of small vessels of $G_{\geq 5}$ in the arterial tree (Parsons et al., 2000a; 2000b). Increased vessel density in response to bFGF and low concentrations of $VEGF_{165}$ represents an acceleration of the ongoing angiogenic process occurring within the CAM. However, the stimulation and inhibition of new, small vessels by bFGF and TGF-β1 was the sole (unimodal) morphological result of cytokine application. Treatment groups appeared to be normally (Gaussian) distributed and were analyzed

by mean and SD with strong statistical confidence. Results for bFGF and TGF-β1 therefore contrast with the non-Gaussian, multimodal response to $VEGF_{165}$ which, except for overall arterial area (Fig. 4), required other kinds of statistical analysis such as scatterplots, ANOVA and Spearman's correlational analysis.

The increase in vascular diameter induced by $VEGF_{165}$ may have resulted from transient vessel dilatation (Neufeld et al., 1999) and/or from the acceleration of ongoing vascular maturation, accompanied by thickening and/or phenotypic change of the mural cell layers (Benjamin et al., 1999; Ozawa et al., 2004). In this study, VEGF appeared to increase the rate of recruitment of αSMA-positive cells to the vascular wall. Vessel diameter increased quickly (within 24 h) and continuously with increasing VEGF concentration (up to 5 μg /CAM). The diameters of larger arteries in $VEGF_{165}$-treated and control specimens at E9 after 48 h of treatment were essentially equivalent (data not shown). VEGF may also have induced the increased expression and activity of nitric oxide (NO), a critical regulator of transient vasodilatation and vasopermeabilization, as indicated by increased vascular leakage in the CAM. It is well-established that VEGF interacts strongly with endothelial and inducible NO synthase (Neufeld et al., 1999).

As revealed by fluorescence IHC, the expression of VEGFR-1 and VEGFR-2 did not change significantly in the CAM following treatment with $VEGF_{165}$, despite strong VEGF stimulation of vascular/lymphatic vessel density and vessel diameter. VEGF receptor expression in the CAM may be regulated by other VEGF's in coordination with VEGF-A, as was found for the tissue-specific, endocrine-gland-derived VEGF, EG-VEGF

(LeCouter et al., 2001). In the CAM, VEGFR-1 was prominently expressed in the capillaries, in a few isolated cells, and weakly lined the surface of smaller blood vessels. VEGFR-2, on the other hand, was strongly expressed on numerous migrating cells that were recruited to the VEGFR-2 positive lymphatics, and to some extent, to smaller blood vessels. The pronounced punctate expression of VEGFR-1 in CAM capillaries, from where the new, small blood vessels emerge, is consistent with the maturational role proposed for VEGFR-1 in formation of blood vessels, in which VEGFR-1 helps to halt vascular growth (Eriksson and Alitalo, 2002; Luttun et al., 2002). Embryonic mice deficient in VEGR-1 die prenatally with excessive numbers of endothelial cells in the vasculature (Fong et al., 1999). In CAM capillaries, VEGFR-1 may also assist in regulation of hematopoietic cell recruitment and mobilization (Hattori et al., 2002).

Precise gradients of VEGF concentration support chemotactic cell migration and are required for correct vascular development *in vivo* (Carmeliet et al., 1996; Ferrara et al., 1996; Ozawa et al., 2004). VEGF gradients supported the filopodial guidance of vascular tip cells expressing VEGFR-2 in the postnatal mouse retina (Gerhardt et al., 2003). We observed intense expression of VEGFR-2 on the filopodia of lymphatic tip cells; strong co-expression of VEGFR-2 and lymphatic-specific VEGFGR-3 was reported by others for developing lymphatics of the quail and chicken CAM (Oh et al., 1997). The switch from VEGF stimulation of increased arterial density to increased arterial diameter (Fig. 3) at higher concentration may result in part from loss of VEGF chemotactic signaling to endothelial migration. VEGF stimulated primarily chemotaxis (the directional component of cell movement) of endothelial cells, whereas bFGF

stimulated primarily chemokinesis (the random component for rate of cell movement) (Yoshida et al., 1996). Protease production was increased by VEGF in migrating human endothelial cells (Ferrara and Davis-Smyth, 1997; Neufeld et al., 1999) and angiogenesis was inhibited by protease-induced blocking of VEGF binding to VEGFR-2 (Qi et al., 2003). Stimulation of protease activity by $VEGF_{165}$ may have contributed to increased tortuosity of small blood vessels in the quail CAM (Fig. 1).

Complex, adaptive biological processes such as angiogenesis and vascular remodeling in the CAM and murine or human retina may be characterized by two types of input signals: (1) complex (or variability-inducing) regulators of divergent outcomes and (2) homeostatic (or variability-reducing) regulators of convergent outcomes (Coffey, 1998; Science, 1999). Small changes in a complex regulator can produce highly variable results that, after some time, may be irreversible. On the other hand, a homeostatic regulator acts to dampen the variability of a response. During angiogenesis, VEGF may act as a complexity regulator by its ability to induce pleiomorphic vascular response. A regulator such as bFGF may act as a homeostatic regulator by increasing only vessel density, thereby suppressing the variation-inducing effects of VEGF activity. The sensitivity of complex biological and physical systems to initial conditions and other important parameters can be surprising. For example, sensitivity analysis showed that lactate metabolism during skeletal muscle glycolysis was affected more by reduction in oxygen delivery than by decrease in tissue oxygen concentration (Radhakrishnan, 1991; Radhakrishnan et al., 2000).

Major angiogenic regulators that induced specific "fingerprint" patterns of vascular perturbation in the quail CAM include the stimulators $VEGF_{165}$ and bFGF and inhibitors angiostatin and TGF-β1. By applying the 2D, region-based fractal methods developed in the quail CAM, we successfully measured the statistically reproducible decrease of vessel density in the human retina during the early nonproliferative phase of diabetic retinopathy, a vascular disease (Avakian et al., 2002). Each vascular tree in a quail CAM specimen or a mammalian retina represents is a unique vascular pattern. Nonetheless, by fractal analysis, the space-filling characteristics of each population group -- including the early-stage human diabetic retina -- were remarkably uniform (Avakian et al., 2002; Parsons et al., 1998). Region-based fractal analysis therefore supports the study of important, emergent properties in highly cooperative, complex systems such as remodeling vasculature that cannot be revealed by molecular reductionist studies alone. (Baish and Jain, 1998; Coffey, 1998).

METHODS AND MATERIALS

Embryonic culture, assay, mounting, imaging, and fractal/VESGEN branching analysis have been described previously (Parsons et al., 1998; 2000a; 2000b).

Culture, Assay and Mounting

Fertilized eggs of Japanese quail (*Coturnix coturnix japonica*, Boyd's Bird Co., Pullman, WA) were incubated at 37.6 ± 0.2 °C under ambient atmosphere, cracked at embryonic day three (E3, following incubation of eggs for 56 hours (h)) and cultured further at the same incubator conditions in petri dishes (cross-sectional area = 10 cm^2). Quail egg culture and experimental methods were approved by the Animal Care Committee, University of Washington, and by the Chief Veterinarian Officer of NASA. At E7 (following incubation for an additional 96 h), 0.5 ml prewarmed PBS solution containing 100 μg/ml ovalbumin (Sigma, albumin chicken egg grade VII) and 0-5 μg human recombinant $VEGF_{165}$ expressed in *E. coli* (G143AB, generous gift of Genentech) was applied dropwise to the surface of each CAM. Because the incubation solution is quickly absorbed into CAM tissue, the total amount of cytokine, rather than cytokine concentration, is the governing parameter and is therefore expressed as μg/CAM. CAM's responded positively to $VEGF_{165}$ from 1-5μg/CAM; embryonic lethality increased at doses ≥ 10 μg/CAM. Results were consistent with those produced by human recombinant $VEGF_{165}$ (293-VE, R & D Systems) expressed in *SF21* insect cells, except that 293-VE $VEGF_{165}$ appeared active at slightly lower concentrations. Following treatment with $VEGF_{165}$ and further incubation for 24 h, the embryos were fixed in either 4% paraformaldehyde/2% glutaraldehyde/PBS for vascular branching analysis or 4% paraformaldehyde/PBS for

fluorescence IHC. Stimulation by $VEGF_{165}$ persisted in specimens treated for 48 h, but was not as strong as stimulation after 24 h.

Quantification of Vascular Branching

Aldehyde fixation of the CAM results in high contrast of the arterial tree, due to retention of erythrocytes (i.e., red blood cells, RBC) within the arteries, and low contrast of the venous tree, due to evacuation of RBC from veins during dissection (Parsons et al., 1998).To support the region-based fractal/VESGEN analysis of arterial change, digital images (640 × 480 pixels) of arterial endpoint vessels from the middle region of the CAM were acquired by the Apple Video Player framegrabber in grayscale (0-255 intensity) at a total magnification of 10x and resolution of 13 μm/pixel with a Nikon Microphot-SA microscope attached to a CCD camera (DEI-470, Optronics). There was no significant increase in vascular density at a total magnification of 20x in comparison with 10x. The images were processed with NIH Image software (http://rsb.info.nih.gov/nih-image/). A square region of 480 × 480 pixels was extracted from the original image, rescaled to a TIFF image of 514 × 514 pixels (to support fractal analysis), binarized to black/white and skeletonized (linearized). The fractal dimension (D_f) was estimated for binary and skeletonized vessels in an image with a MATLAB-supported computer program (available from corresponding author) implementing a box-counting algorithm (Parsons et al., 1998). The box-counting method for measuring D_f is now available in NIH Image J.

Vessel diameter (not vessel length or branching angle) is the strongest correlate of vessel branching generation in 3D arterial and venous trees of the mammalian heart and lung (Gan et al., 1993; Kassab et al., 1994; Kassab et al., 1993), in which the most

frequent branching event is nonequivalent branching (i.e., branching of a smaller vessel from a much larger vessel), not equivalent or symmetric branching (branching of a parent vessel into two equal offspring vessels). The CAM is in many respects a functional and morphological analog of the lung. For generational analysis of vascular branching by the computer program VESGEN (Fig. 2), vessels were first classified according to proportional decrease in vessel diameter (Parsons et al., 2000a; 2000b). VESGEN is available as a MATLAB-supported program from the corresponding author, and is currently being developed by NASA as a user-interactive (GUI-supported), MATLAB-independent computer code. The largest arterial tree was extracted from a processed binary image and the single parent vessel (the vessel of largest diameter) was designated as the first generation (G_1). Vessels of G_5 or greater were lumped into a single generational parameter ($G_{\geq 5}$), because of limiting resolution for accurate measurement.

Parameters of vessel length density (L_v), vessel area density (A_v) and vessel number density (N_v) were measured for each branching generation G_1 through $G_{\geq 5}$. Average vessel diameter (D_v) was calculated as $D_v = A_v/L_v$. For example, $D_{v1\text{-}3}$ denotes D_v with respect to the specific generations, G1-G3. L_v, A_v and N_v were expressed as density functions by normalization to either the CAM surface area that is occupied by the extracted arterial tree (Fig. 1) or the entire image, rather than in single extracted vascular trees that occupied approximately 40-80% of the total area of the source images.

Forty-five representative CAM specimens was quantified from four independent experiments. Additional specimens and experiments served as qualitative confirmation of quantified results. Results for A_v, L_v, D_v and D_f were compared among the five

treatment groups (0-5 μg $VEGF_{165}$/CAM) by single-factor analysis of variance (ANOVA). Response to VEGF treatment was not normally distributed (i.e., was non-Gaussian) for L_v and D_v, unlike control groups. Hence specimens in VEGF treatment groups were classified as responders or non-responders by a simple cutoff criterion: Responders displayed values > $(\text{mean} + \text{SD})_{\text{control}}$ and non-responders, ≤ $(\text{mean} + \text{SD})_{\text{control}}$. Correlation between L_v and D_v was tested yielded Spearman's rank coefficient r_S using SPSS 8.0 software.

Fluorescence Immunohistochemistry

Polyclonal, affinity-purified IgG antisera were applied to CAM specimens by conventional whole-mount fluorescence IHC (Drake and Little, 1995; Parsons et al., 2000b). Staining for nonspecific IgG controls in the IHC was low, and observations were made from a number of experiments. VEGFR-1 was identified primarily by goat sc-316g, and confirmed by rabbit sc-316 (1:200 dilution, proprietary epitope from c-terminus of human VEGFR-1, Santa Cruz Biotechnology). VEGFR-2 was identified by RB-1526 (1:200 dilution, epitope from aa 1326-1345, c-terminus of mouse Flk-1 precursor; Lab Vision). The QH-1 monoclonal antibody (mouse ascites diluted 1:1000, Development Studies Hybridoma Bank, University of Iowa) specifically recognizes quail vasculature and an unidentified hematopoietic precursor cell (Coffin and Poole, 1991; Pardanaud et al., 1987). Fluorescently labeled secondary antibodies conjugated to Alexa Fluor 488 and 568 were obtained from Molecular Probes, and secondary antibodies conjugated to Cy3 and Cy5, from Jackson Immunoresearch. Nuclei were

labeled with Hoechst 33342 (Molecular Probes MP H-3570). We tested three antibodies recognizing VEGFR-3, but found they were negative in the quail CAM.

After fixation with 4% paraformaldehyde/PBS at 4°C for 48 h at E6-E7 and 24 h at E8-E9, specimens were blocked in 5% normal donkey serum (NDS)/1% Triton X-100/PBS, and incubated overnight at 4°C with primary antibody at 1:200 dilution in 0.2% NDS/PBS (except for RB-1526, incubated for 2 hours the following day), followed by incubation with secondary antibodies and mounting with 50% polyvinyl alcohol (PVA)/glycerol solution (Parsons et al., 1998), and 50% Vectashield™ (Vector Labs). Specimens were imaged with a Leica DM-RXE confocal microscope with TCS-SP2 scanner/Leica confocal software version 2.5 or a Leica DM-R fluorescence microscope with Micromax CCD-1300-V camera, Princeton Instruments and Image-Pro Plus Version 4.1.1.2 software. Volocity software (Improvision) was used for 3D reconstruction of confocal z-series images. Confocal images at 633X total magnification from specimens treated with VEGFR-2 antiserum RB-1526 were post-processed in Adobe Photoshop CS (version 8.0) to remove nonspecific background.

ACKNOWLEDGEMENTS

The authors gratefully acknowledge electrical engineering undergraduate student Van Le Thuy for excellent image processing and fractal analysis; Terence Condrich, John Jindra, Lisa Liuzzo and Mary Eitel-Kim, NASA Glenn Publication Services, for expert figure preparation; Judy Drazba, Cleveland Clinic Foundation, for helpful consultation on fluorescence imaging and histology, and Helene Sage, Hope Heart Institute, in whose laboratory some of the experiments were performed. We thank Robert Hendricks, Terri McKay and Sandra Olson, NASA Glenn, and Elaine Raines, Department of Pathology and the Department of Biostatistics, University of Washington, and Alanna Ruddell, Fred Hutchinson Cancer Research Center, for consultation and/or reading of the manuscript. The research was supported by Internal Research and Development Award (IRD04-54), Commercial Technology Office awards NCC3-622, NCC3-782 and NCC3-912, BioScience and Engineering/Fluid Physics, John Glenn Research Center, National Aeronautics and Space Administration (NASA); National Science Foundation Grant EEC-9529161 to the University of Washington Engineered Biomaterials (UWEB) and National Institutes of Health Grant GM-40711.

ABBREVIATIONS

bFGF, basic fibroblast growth factor (fibroblast growth factor-2); CAM, chorioallantoic membrane; immunohistochemistry, IHC; TGF-β1, transforming growth factor beta-1; VEGF, vascular endothelial growth factor; VEGFR, vascular endothelial growth factor receptor.

FIGURES

Fig. 1. Regulation of Multimodal Arterial Change by $VEGF_{165}$.

$VEGF_{165}$ stimulated several morphological changes in CAM specimens treated at E7 for 24 h, illustrated by representative binary and skeletonized (linearized) images of arterial endpoints. Relative to control specimens (**A**, **E**), increased arterial density (**B**, **F**) is associated with low VEGF concentration (1.25-2.5 μg/CAM) and increased arterial diameter (**C**, **G**), with high concentration (2.5-5 μg/CAM). Some specimens display both increased arterial density and increased arterial diameter (**D**, **H**). Vessel area density (A_v), vessel length density (L_v) and the fractal dimension (D_f) are given. Treatment with $VEGF_{165}$ frequently resulted in the increased tortuosity of small arteries (**D**, **H**) and increased vascular leakage (associated with increased vessel diameter, results not shown).

Fig. 2. Generational Branching in the Arterial Tree of the Quail CAM.

A pseudocolor image of a CAM arterial tree from a control specimen fixed at E8 illustrates the classification of vessel branching generation (G_1 through $G_{\geq 5}$) according to relative decreases in vessel diameter (D_v), as first established in the dog and pig heart and lung (Gan et al., 1993; Kassab et al., 1994; Kassab et al., 1993). The major arterial tree was extracted from a binary image such as Fig. 1A-D for analysis by the computer program VESGEN. The schematic depicts the area occupied by the tree used to calculate the density of vessel parameters that include area (A_v), length (L_v), number (N_v) and branchpoint (B_v). Parameters are further specified to specific

generations such as D_{v1-3}. The area of normalization is enclosed by the black line lying midway between the arterial endpoints of the tree and neighboring arteries. In regions where vessels of the arterial tree extend beyond the edge of the image, the area of normalization was defined simply by the edge of the image.

Fig. 3. Arterial Density and Arterial Diameter Increase Independently in Response to $VEGF_{165}$. (**A**) The relative frequency (%) of responders for arterial density measured by fractal dimension D_f in skeletonized images and for arterial diameter by D_{v1-3} in binary images are plotted as functions of increasing $VEGF_{165}$. Responder frequency was determined by a simple statistical cutoff test as illustrated (**B**-**C**). A specimen was counted as a responder if D_f or $D_{v1-3} \geq$ (mean + SD) of the control group, denoted by the horizontal line and vertical error bar. (**B**) The frequency of response for D_f to $VEGF_{165}$ was highest at 1.25 μg/CAM. Numerical labels (such as 6/9) denote the number of responder specimens (numerator) compared to the total number of specimens in the treatment group (denominator). Overlapping data points are displayed to right, and if necessary to left, of data column. (**C**) Response of arterial diameter in branching generations D_{v1-3} increased with increasing concentration of $VEGF_{165}$.

Fig. 4. Regulation of Overall Arterial Area by $VEGF_{165}$. Increased arterial area density A_v in binary arterial images (Fig. 1A-D) can result from either increased vessel density and/or increased vessel diameter. (**A, B**) By A_v, arterial area increased in

response to increasing concentration of VEGF (confirmed by ANOVA, Table 1). The relative frequency (%) of responders in responding treatment groups by A_v was essentially constant, despite differing trends for increased vessel density and diameter (Figs. 1, 3).

Fig. 5. Reciprocal Expression of VEGFR-1 and VEGFR-2. (**A-D**) By IHC of control specimens at E8, the vascular marker QH-1 (**A**) and VEGFR-2 (**B**) were essentially co-localized. QH-1 and VEGFR-2 were expressed most intensely on lymphatic vessels (large lymphatic plexus surrounding large blood vessel, arrowhead; smaller lymphatic vessel adjacent to smaller blood vessels, arrow) and in single isolated cells (hollow arrow). Moderate to low expression was present on blood vessels and capillaries. VEGFR-1 expression (red, **C**- **G**) was generally reciprocal to VEGFR-2 (**B**) and QH-1 (**A**, **D**). VEGFR-1 was localized primarily to the capillary lumen in a punctate fashion, was present in moderate abundance on some smaller blood vessels, and was absent from lymphatic vessels and from most isolated cells. Relative to untreated controls (**D**, **E**), VEGFR-1 expression was not significantly altered in response to application of $VEGF_{165}$ at 1.25 μg /CAM (**F**) and 5 μg/CAM (**G**). **A-G**: All confocal images.

Fig. 6. $VEGF_{165}$ Increases the Diameter and Density of Lymphatic Vessels, and Induces Lymphatic Dissociation from Blood Vessels.

(**A**, **C-E**) By IHC of VEGFR-2 (green) and QH-1 (red) relative to control specimens (**A**), lymphatic vessels (arrowheads) enlarged and dissociated from blood vessels (arrows) in response to the application of $VEGF_{165}$ at 1.25 μg/CAM (**C**) and 5 μg/CAM (**D**). (**E**) The lymphatics frequently reassociated as a network (hollow arrowhead) when treated with 1.25 or 5 μg VEGF/CAM, which is a regression of lymphatic morphology to that observed in the normal CAM at E5-E6 (**B**, visualized by QH-1). (**A**,**C-E**) Note large numbers of single, isolated cells co-expressing VEGFR-2 and QH-1. **A**, **C-E**: Confocal images. **B**: Fluorescence image.

Fig. 7. $VEGF_{165}$ Increases Vessel Density During Angiogenesis by Vascular Expansion from the Capillary Network.

(**A**,**C**) In control specimens expressing αSMA at E8, post-capillary venules (PCV, arrowheads) and an arteriole (arrow) emerge from the capillary network, displaying increasingly large round gaps compared to smaller round gaps of the intercapillary spaces. Staining for αSMA clearly delineating the round capillary gaps is transitory and no longer visible in the mature capillaries at E9 - E10 (results not shown). (**B**) Fine processes (arrowhead) of αSMA, an enlarged detail from PCV (**A**, arrowhead) span the distance between two neighboring gaps of the PCV emerging from the capillary bed. (**D**) Following application of $VEGF_{165}$ at 1.25 μg/CAM, blood vessels displayed more frequent, abnormal anastomoses (arrowhead) relative to controls (**A**, **C**). (**E**) At E6 in untreated controls, many single cells expressing αSMA are merging with blood vessels (arrowheads). Compared to E6, merging of αSMA-positive cells with blood vessels

(arrowheads) at E8 was observed with decreased frequency in control specimens (**F**) or with similar frequency in VEGF-treated specimens (**G**). **A**-**D**,**G**: Fluorescence images. **E**,**F**: Confocal images.

Fig. 8. $VEGF_{165}$ Stimulates Lymphangiogenesis, but not Angiogenesis, by Cell Recruitment to the Tips of Sprouting Vessels.

By IHC of control specimen at E7 expressing (**A**) αSMA and (**B**) QH-1 (co-localized with VEGFR-2), small blood vessels (arrowheads) emerge directly from the capillary network. This field (**A**, **B**) is a small region (**C**, arrowhead) adjacent to a larger blood vessel enclosed by a lymphatic network containing numerous blind-ended lymphatic sprouts. (**D**) At higher magnification, lymphatic sprouts led by tip cells with filopodia (arrowhead) are visible. (**E**,**F**) Filopodial processes of lymphatic tip cells (arrowhead) are clearly shown. The lymphatic tip cells are details from a well-developed lymphatic network enclosing a large blood vessel, as shown at lower magnification in **C** - **D**. (**G**, **H**) In specimens treated with $VEGF_{165}$ at 1.25 μg/CAM, the small, anastomotic blood vessels emerge directly from the capillary network (arrowhead). (**I**) In the thickened lymphatic network enclosing a large blood vessel from a more mature control specimen at E9, lymphatic sprouts with tip cells displaying filopodia are still present.

Fig. 9. Model of Angiogenic Expansion and Lymphatic Sprouting as Stimulated by $VEGF_{165}$ in the CAM. (**A**) ***Angiogenic Expansion***: At E6 - E8, the capillary network and vascular tree are actively developing in response to

stimulation by $VEGF_{165}$ and ongoing angiogenesis. Migrating cells positive for αSMA are frequently recruited to growing blood vessels, and the highly plastic capillaries are temporarily positive for αSMA. Small new arterioles and post-capillary venules (PCV) arise out of the capillary network and display an increasing gap size in the smooth muscle layer. (**B**) The round gaps of smooth muscle become less prominent as blood vessels enlarge and mature, and the precursor cells positive for αSMA or VEGFR-2 disappear. (**C**) ***Lymphatic Sprouting:*** The growing lymphatic network, which is relatively homogeneous at E6, differentiates by attaching and growing as prominent networks around large blood vessels, and as loosely associated vessels around smaller blood vessels. The lymphatics, which are strongly positive for VEGFR-2 and negative for αSMA, recruit VEGFR-2 expressing cells to the tips of blind-ended sprouts on vessels and in networks. (**D**) As a detail of (**C**), tip cells display numerous, prominent filopodia, most of which later fuse with the growing lymphatic vessel.

TABLES

Table 1. ANOVA Analysis of Vascular Response to $VEGF_{165}$ in Arterial Endpoints of Quail CAM.

Results for A_v and D_f (from binary images) and L_v and D_f (from skeletonized images) were analyzed by ANOVA for groups treated with 0-5 $VEGF_{165}$ μg/CAM. Input groups are separated by commas; treatment groups lumped together as a single input group are connected by a hyphen, and *n* indicates the number of samples per input group.

Input Groups (by treatment with μg $VEGF_{165}$/CAM)	*p*-value (α = 0.05)		Conclusion (i.e., relationship among groups)
	A_v L_v (cm^{-1}) D_{v1-3}	D_f (binary) D_f (skeletonized)	
0, 0.5, 1.25, 2.5, 5 (*n* = 9, 7, 9, 10, 10)	0.001 0.22 0.01	0.002 0.18	highly different different highly different
0-0.5, 1.25-5 (*n* = 16, 29)	0.00002 0.03 0.01	0.002 0.02	highly different highly different highly different
0, 0.5 (*n* = 9, 7)	0.64 0.46 0.72	0.54 0.48	inconclusive inconclusive inconclusive
1.25, 2.5, 5 (*n* = 9, 10, 10)	0.87 0.43 0.14	0.86 0.74	similar inconclusive different
1.25, 2.5 (*n* = 9, 10)	0.61 0.96 0.14	0.59 0.98	similar highly similar different
2.5, 5 (*n* = 10, 10)	0.94 0.55	0.89 0.46	highly similar inconclusive

REFERENCES

Argraves, W.S., A.C. Larue, P.A. Fleming, and C.J. Drake. 2002. VEGF signaling is required for the assembly but not the maintenance of embryonic blood vessels. *Dev. Dyn.* 225:298-304.

Avakian, A., R.E. Kalina, E.H. Sage, A.H. Rambhia, K.E. Elliott, E.L. Chuang, J.I. Clark, J.-N. Hwang, and P. Parsons-Wingerter. 2002. Fractal analysis of region-based vascular change in the normal and non-proliferative diabetic retina. *Curr Eye Res.* 24:274-280.

Baish, J.W., and R.K. Jain. 1998. Cancer, angiogenesis and fractals [letter]. *Nat Med.* 4:984.

Benjamin, L.E., D. Golijanin, A. Itin, D. Pode, and E. Keshet. 1999. Selective ablation of immature blood vessels in established human tumors follows vascular endothelial growth factor withdrawal. *J. Clin. Invest.* 103:159-165.

Benjamin, L.E., I. Hemo, and E. Keshet. 1998. A plasticity window for blood vessel remodelling is defined by pericyte coverage of the preformed endothelial network and is regulated by PDGF-B and VEGF. *Development*. 125:1591-1598.

Byzova, T.V., C.K. Goldman, J. Jankau, J. Chen, G. Cabrera, M.G. Achen, S.A. Stacker, K.A. Carnevale, M. Siemionow, S.R. Deitcher, and P.E. DiCorleto. 2002. Adenovirus encoding vascular endothelial growth factor-D induces tissue-specific vascular patterns in vivo. *Blood*. 99:4434-4442.

Carmeliet, P., V. Ferreira, G. Breier, S. Pollefeyt, L. Kieckens, M. Gertsenstein, M. Fahrig, A. Vandenhoeck, H. Kendraprasad, C. Eberhardt, C. Declercq, J. Pawling, L. Moons, D. Collen, W. Risau, and A. Nagy. 1996. Abnormal blood vessel development and lethality in embryos lacking a single VEGF allele. *Nature.* 380:435-439.

Coffey, D.S. 1998. Self-organization, complexity and chaos: the new biology for medicine. *Nat. Med.* 4:882-5.

Coffin, J.D., and T.J. Poole. 1991. Endothelial Cell Origin and Migration in Embryonic Heart and Cranial Blood Vessel Development. *Anat. Rec.* 231:383-395.

Drake, C.J., and C.D. Little. 1995. Exogenous vascular endothelial growth factor induces malformed and hyperfused vessels during embryonic neovascularization. *Proc. Natl. Acad. Sci. USA*. 92:7657-7661.

Eriksson, U., and K. Alitalo. 2002. VEGF receptor 1 stimulates stem-cell recruitment and new hope for angiogenesis therapies. *Nat. Med.* 8:775-777.

Ferrara, N., K. Carver-Moore, H. Chen, M. Dowd, L. Lu, K.S. O'Shea, L. Powell-Braxton, K.J. Hillan, and M.W. Moore. 1996. Heterozygous embryonic lethality induced by targeted inactivation of the VEGF gene. *Nature.* 380:439-442.

Ferrara, N., and T. Davis-Smyth. 1997. The biology of vascular endothelial growth factor. *Endocr. Rev.* 18:4-25.

Ferrara, N., H.P. Gerber, and J. LeCouter. 2003. The biology of VEGF and its receptors. *Nat. Med.* 9:669-676.

Fong, G.H., L. Zhang, D.M. Bryce, and J. Peng. 1999. Increased hemangioblast commitment, not vascular disorganization, is the primary defect in flt-1 knock-out mice. *Development*. 126:3015-3025.

Gan, R.Z., Y. Tian, R.T. Yen, and G.S. Kassab. 1993. Morphometry of the dog pulmonary venous tree. *J. Appl. Physiol.* 75:432-40.

Gerhardt, H., M. Golding, M. Fruttiger, C. Ruhrberg, A. Lundkvist, A. Abramsson, M. Jeltsch, C. Mitchell, K. Alitalo, D. Shima, and C. Betsholtz. 2003. VEGF guides angiogenic sprouting utilizing endothelial tip cell filopodia. *J. Cell Biol.* 161:1163-1177.

Hattori, K., B. Heissig, Y. Wu, S. Dias, R. Tejada, B. Ferris, D.J. Hicklin, Z. Zhu, P. Bohlen, L. Witte, J. Hendrikx, N.R. Hackett, C.R. G., M.A. Moore, Z. Werb, D. Lyden, and S. Rafii. 2002. Placental growth factor reconstitutes hematopoiesis by recruiting VEGFR1(+) cells from bone-marrow miroenvironment. *Nat. Med.* 8:841-849.

Kassab, G.S., D.H. Lin, and Y.C. Fung. 1994. Morphometry of pig coronary venous system. *Am. J. Physiol.* 267:H2100-13.

Kassab, G.S., C.A. Rider, N.J. Tang, and Y.C. Fung. 1993. Morphometry of pig coronary arterial trees. *Am. J. Physiol.* 265:H350-65.

LeCouter, J., J. Kowalski, J. Foster, P. Hass, Z. Zhang, L. Dillard-Telm, G. Frantz, L. Rangell, L. DeGuzman, G.-A. Keller, F. Peale, A. Gurney, K.J. Hillan, and N. Ferrara. 2001. Identification of an angiogenic mitogen selective for endocrine gland endothelium. *Nature.* 412:877-884.

Luttun, A., M. Tjwa, L. Moons, Y. Wu, A. Angelillo-Scherrer, F. Liao, J.A. Nagy, A. Hooper, J. Priller, B. De Klerck, V. Compernolle, E. Daci, P. Bohlen, M. Dewerchin, J.-M. Herbert, R. Fava, P. Matthys, G. Carmeliet, D. Collen, D.H. F., D.J. Hicklin,

and P. Carmeliet. 2002. Revascularization of ischemic tissues by PlGF treatment, and inhibition of tumor angiogenesis, arthritis and atherosclerosis by anti-Flt1. *Nat. Med.* 8:831-840.

Mandelbrot, B.B. 1983. *The Fractal Geometry of Nature.* W. H. Freeman, San Francisco.

Nagy, J.A., A.M. Dvorak, and H.F. Dvorak. 2003. VEGF-A(164/165) and PlGF: roles in angiogenesis and arteriogenesis. *Trends Cardiovasc. Med*. 13:169-175.

Neufeld, G., T. Cohen, S. Gengrinovitch, and Z. Poltorak. 1999. Vascular endothelial growth factor (VEGF) and its receptors. *FASEB J.* 10:9-22.

Oh, S.J., M.M. Jeltsch, R. Birkenhager, J.E. McCarthy, H.A. Weich, B. Christ, K. Alitalo, and J. Wilting. 1997. VEGF and VEGF-C: specific induction of angiogenesis and lymphangiogenesis in the differentiated avian chorioallantoic membrane. *Dev. Biol.* 188:96-109.

Ozawa, C.R., A. Banfi, N.L. Glazer, G. Thurston, M.L. Springer, P.E. Kraft, D.M. McDonald, and H.M. Blau. 2004. Microenvironmental VEGF concentration, not total dose, determines a threshold betwen normal and aberrant angiogenesis. *J. Clin. Invest.* 113:516-527.

Pardanaud, L., C. Altman, P. Kitos, F. Dieterlen-Lievre, and C.A. Buck. 1987. Vasculogenesis in the early quail blastodisc as studied with a monoclonal antibody recognizing endothelial cells. *Development*. 100:339-349.

Parsons-Wingerter, P., K.E. Elliott, J.I. Clark, and A.G. Farr. 2000b. Fibroblast growth factor-2 selectively stimulates angiogenesis of small vessels in arterial tree. *Arterioscler. Thromb. Vasc. Biol.* 20:1250-1256.

Parsons-Wingerter, P., K.E. Elliott, A.G. Farr, K. Radhakrishnan, J.I. Clark, and E.H. Sage. 2000a. Generational analysis reveals that TGF-beta1 inhibits the rate of angiogenesis in vivo by selective decrease in the number of new vessels. *Microvasc. Res*. 59:221-232.

Parsons-Wingerter, P., B. Lwai, M.C. Yang, K.E. Elliott, A. Milaninia, A. Redlitz, J.I. Clark, and E.H. Sage. 1998. A novel assay of angiogenesis in the quail chorioallantoic membrane: stimulation by bFGF and inhibition by angiostatin according to fractal dimension and grid intersection. *Microvasc. Res.* 55:201-14.

Qi, J.H., Q. Ebrahem, N. Moore, G. Murphy, L. Claesson-Welsh, M. Bond, A. Baker, and B. Anand-Apte. 2003. A novel function for tissue inhibitor of metalloproteinases-3 (TIMP3): inhibition of angiogenesis by blockage of VEGF binding to VEGF receptor-2. *Nat Med.* 9:407-415.

Radhakrishnan, K. 1991. Combustion Kinetics and Sensitivity Analysis Computations. In *Numerical Approaches to Combustion Modeling*. E. Oran and J. Boris, editors. AIAA, Washington, D.C. 83-128.

Radhakrishnan, K., J.C. LaManna, and M.E. Cabrera. 2000. A Quantitative Study of Oxygen as a Metabolic Regulator. *Appl Cardiopulmonary Pathophysiol*. 9:363-367.

Risau, W., and I. Flamme. 1995. Vasculogenesis. *Ann. Rev. Cell Dev. Biol.* 11:73-91.

Science. 1999. Complex Systems (Special Section). 284:79-109.

Yoshida, A., B. Anand-Apte, and B.R. Zetter. 1996. Differential endothelial migration and proliferation to basic fibroblast growth factor and vascular endothelial growth factor. *Growth Factors.* 13:57-64.

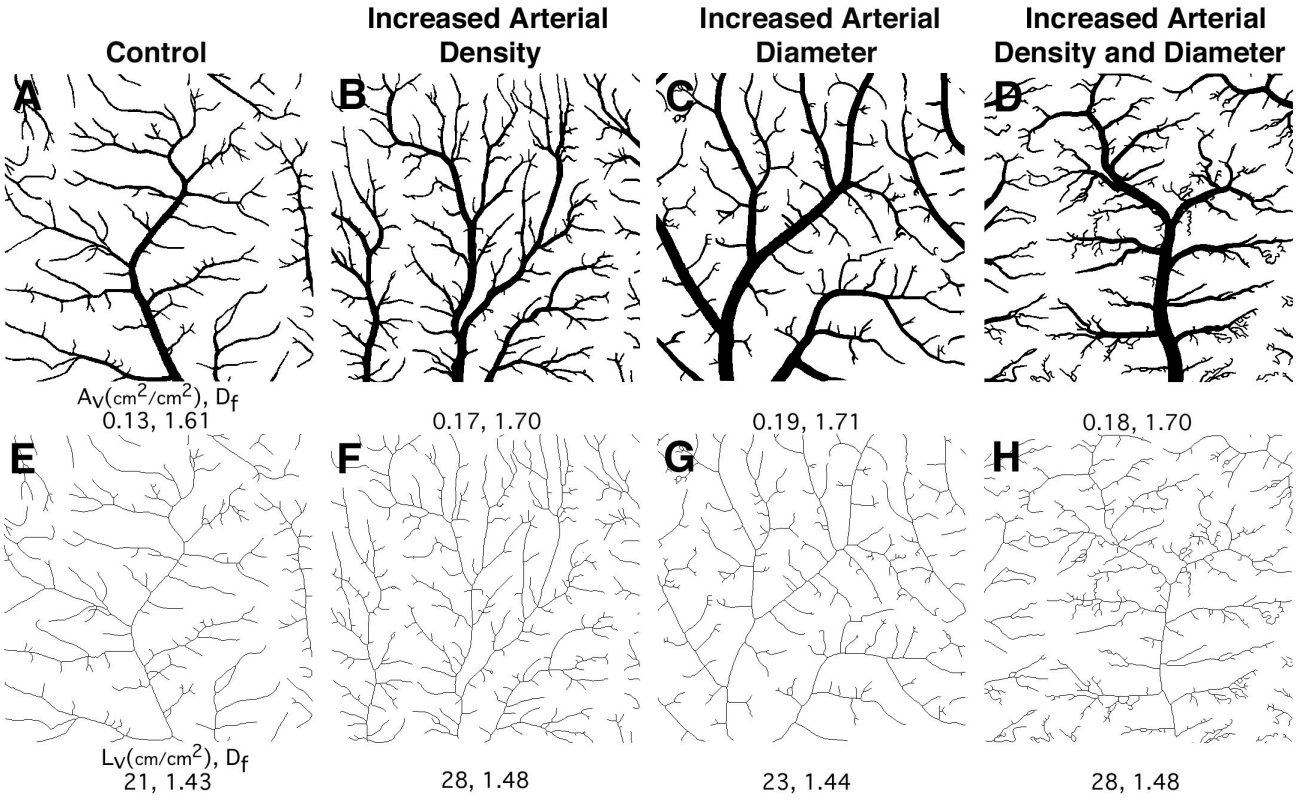

Fig. 1. Parsons-Wingerter *et al*.

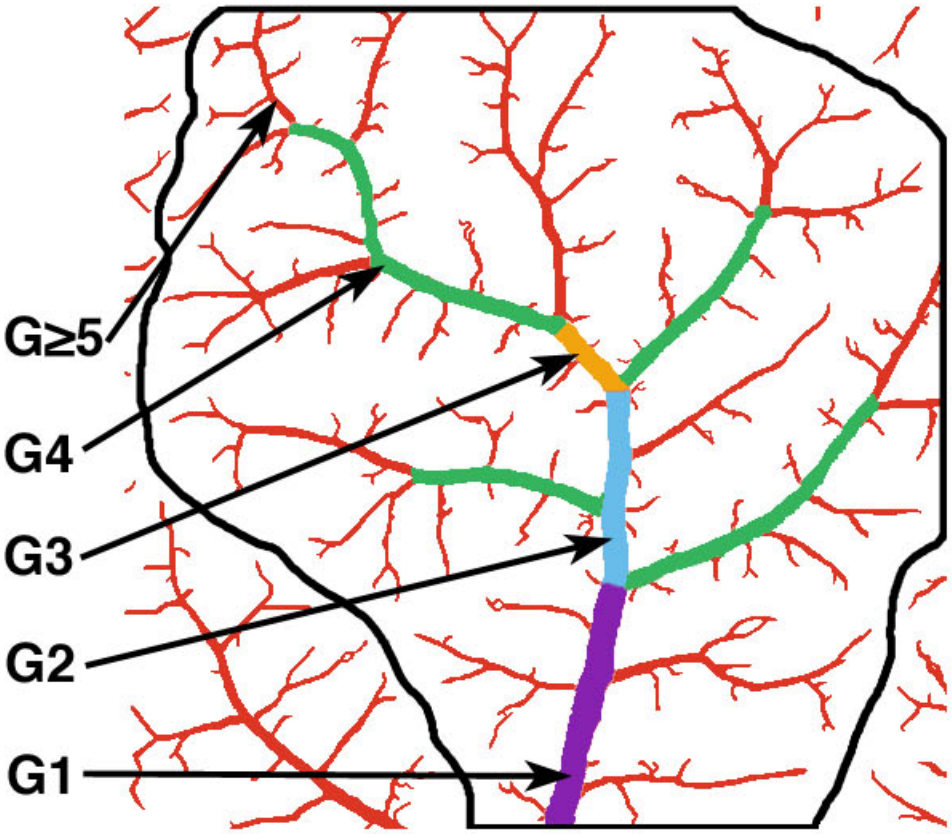

Fig. 2. Parsons-Wingerter *et al.*

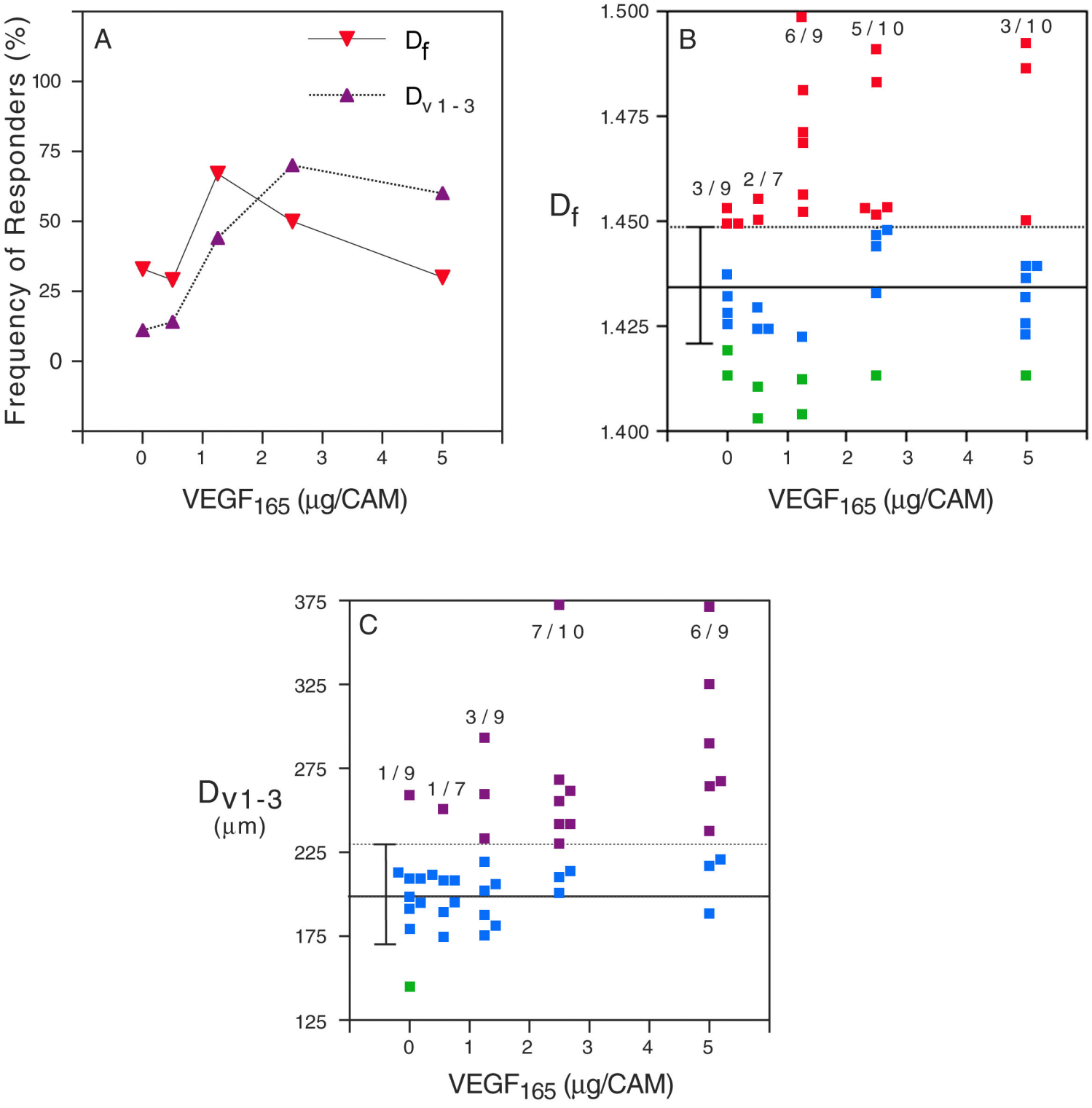

Fig. 3. Parsons-Wingerter *et al.*

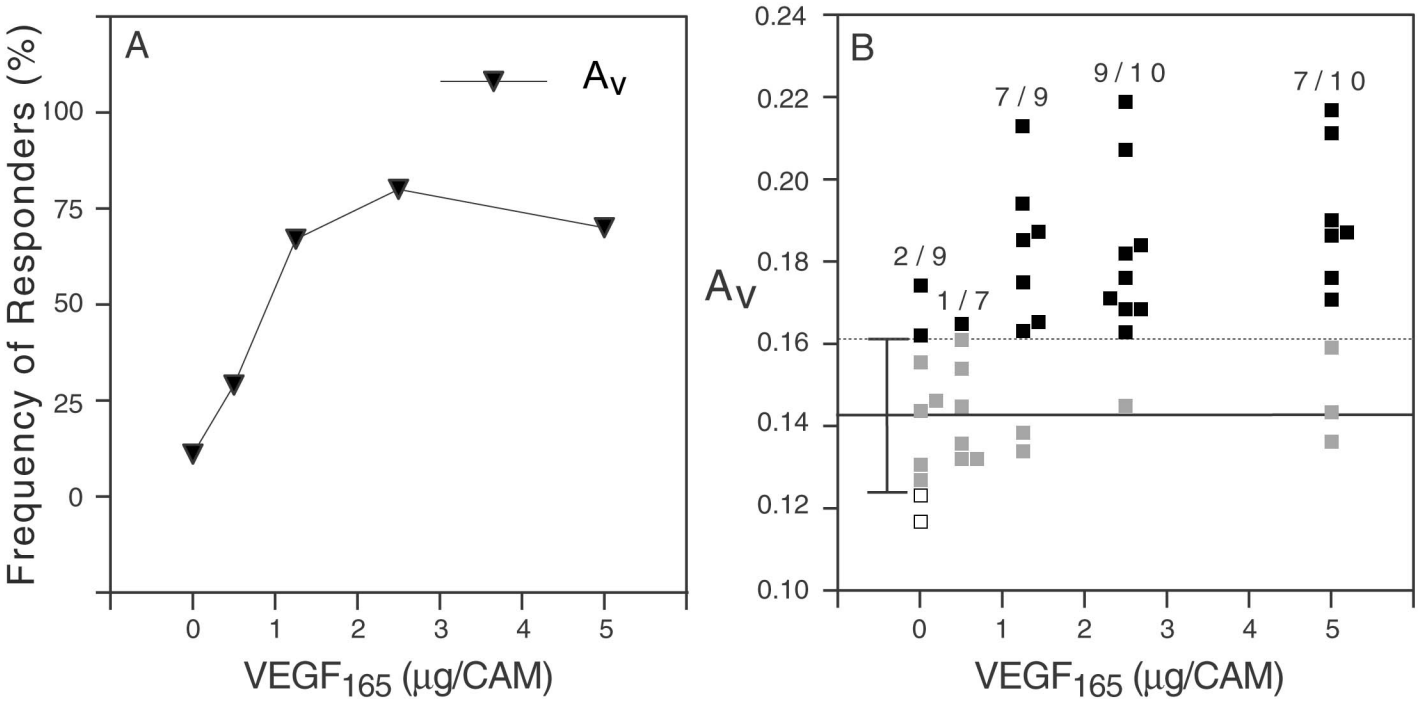

Fig. 4. Parsons-Wingerter *et al.*

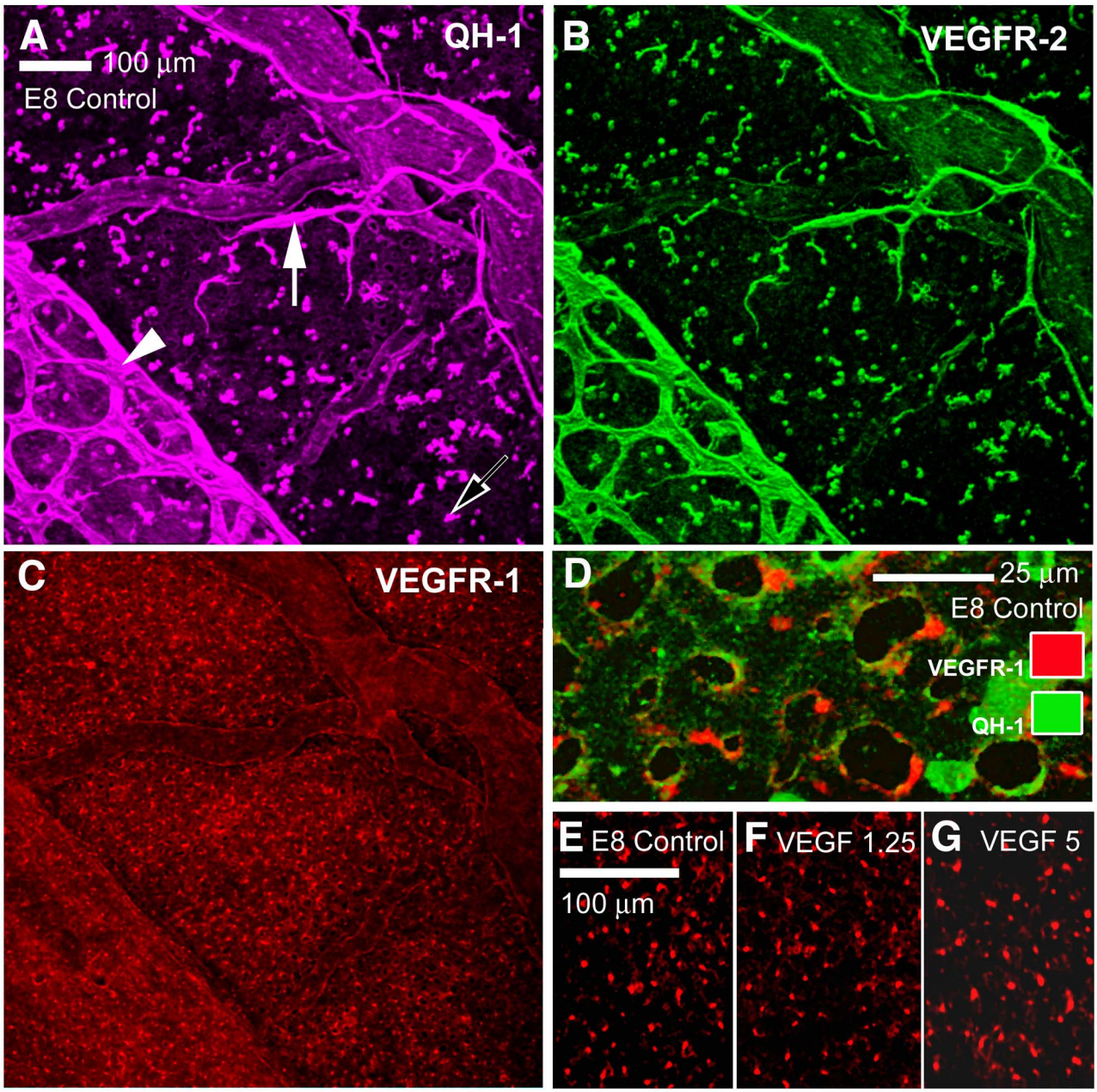

Fig. 5. Parsons-Wingerter *et al.*

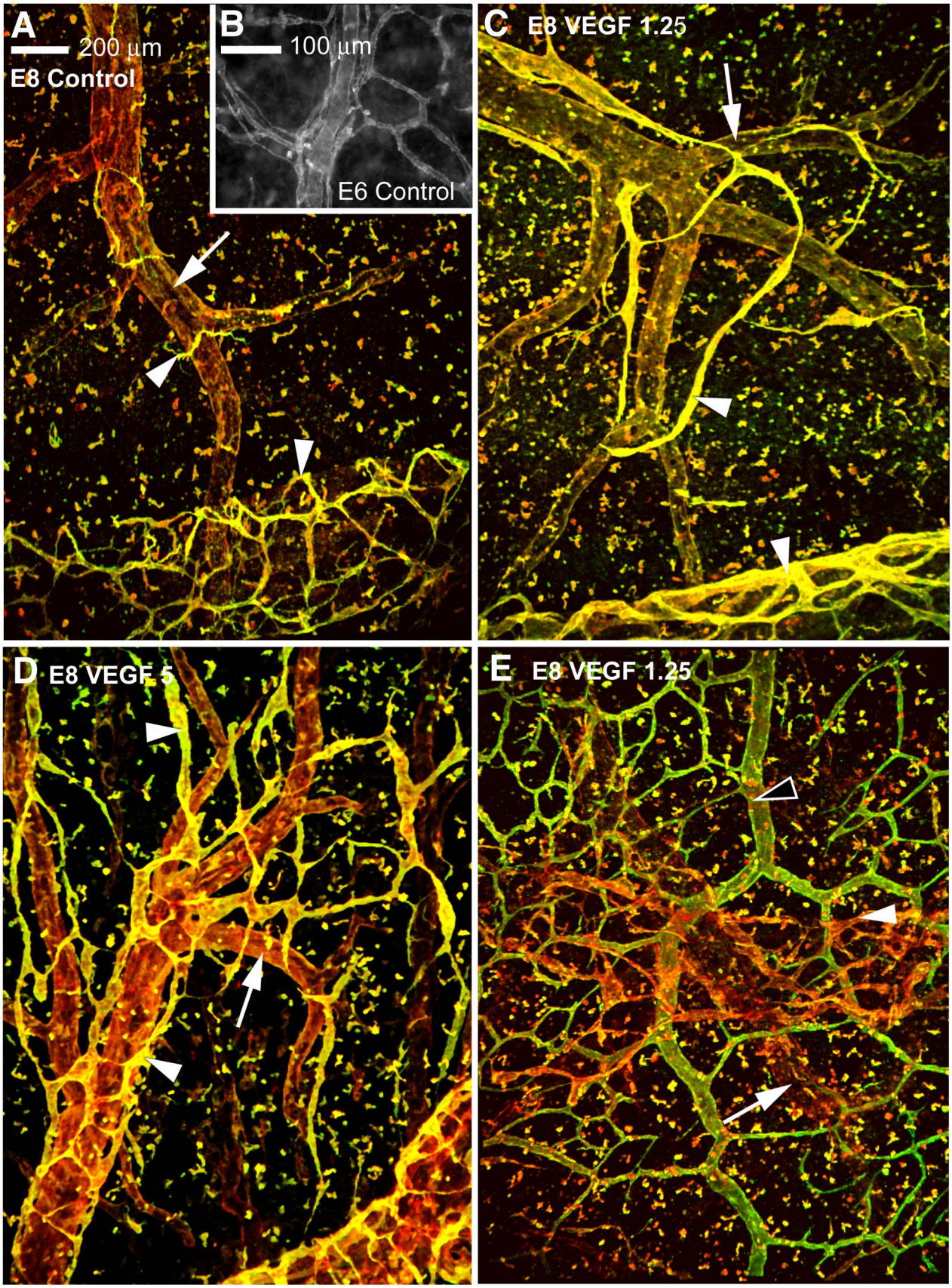

Fig. 6. Parsons-Wingerter *et al.*

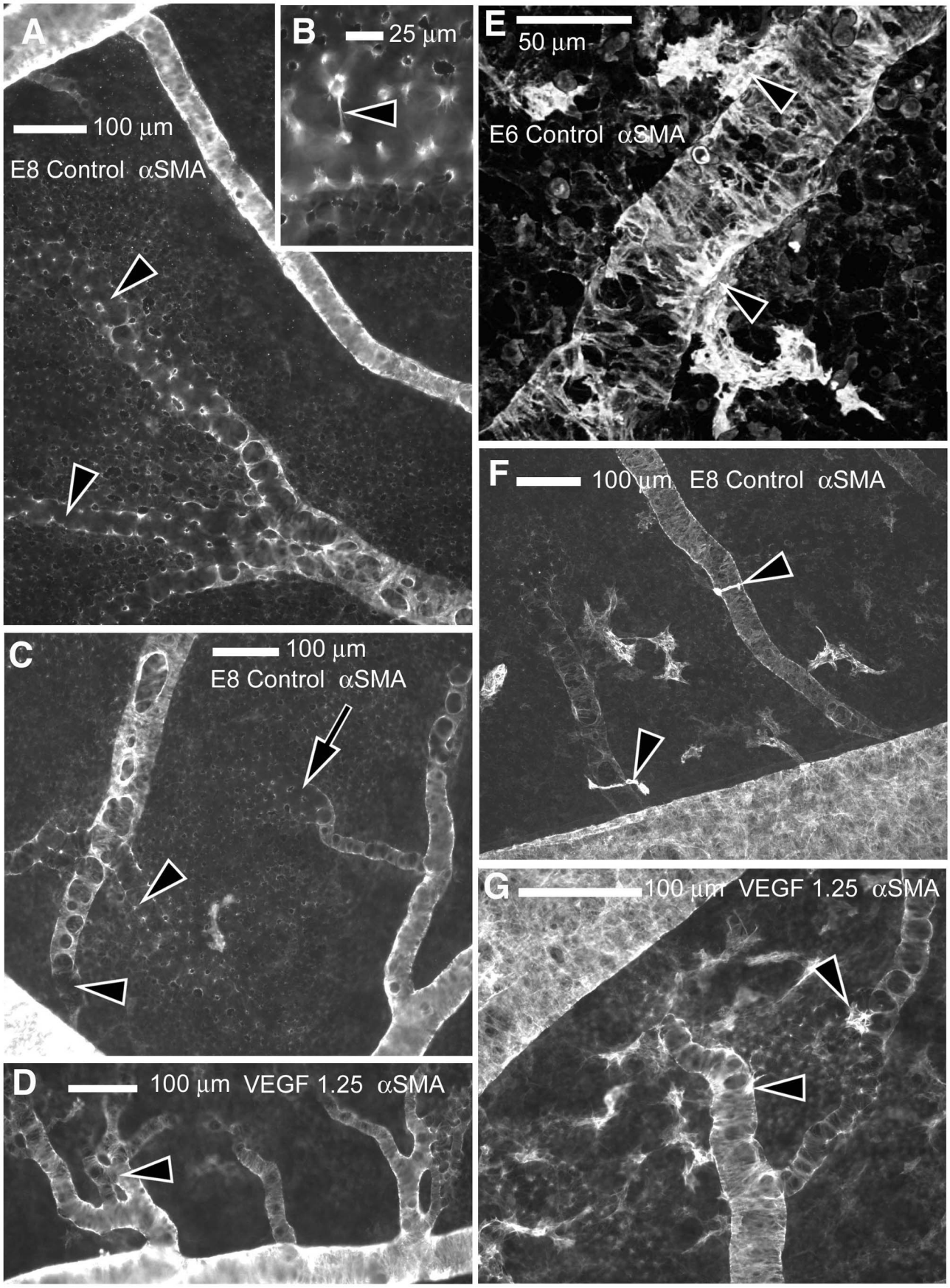

Fig. 7. Parsons-Wingerter *et al.*

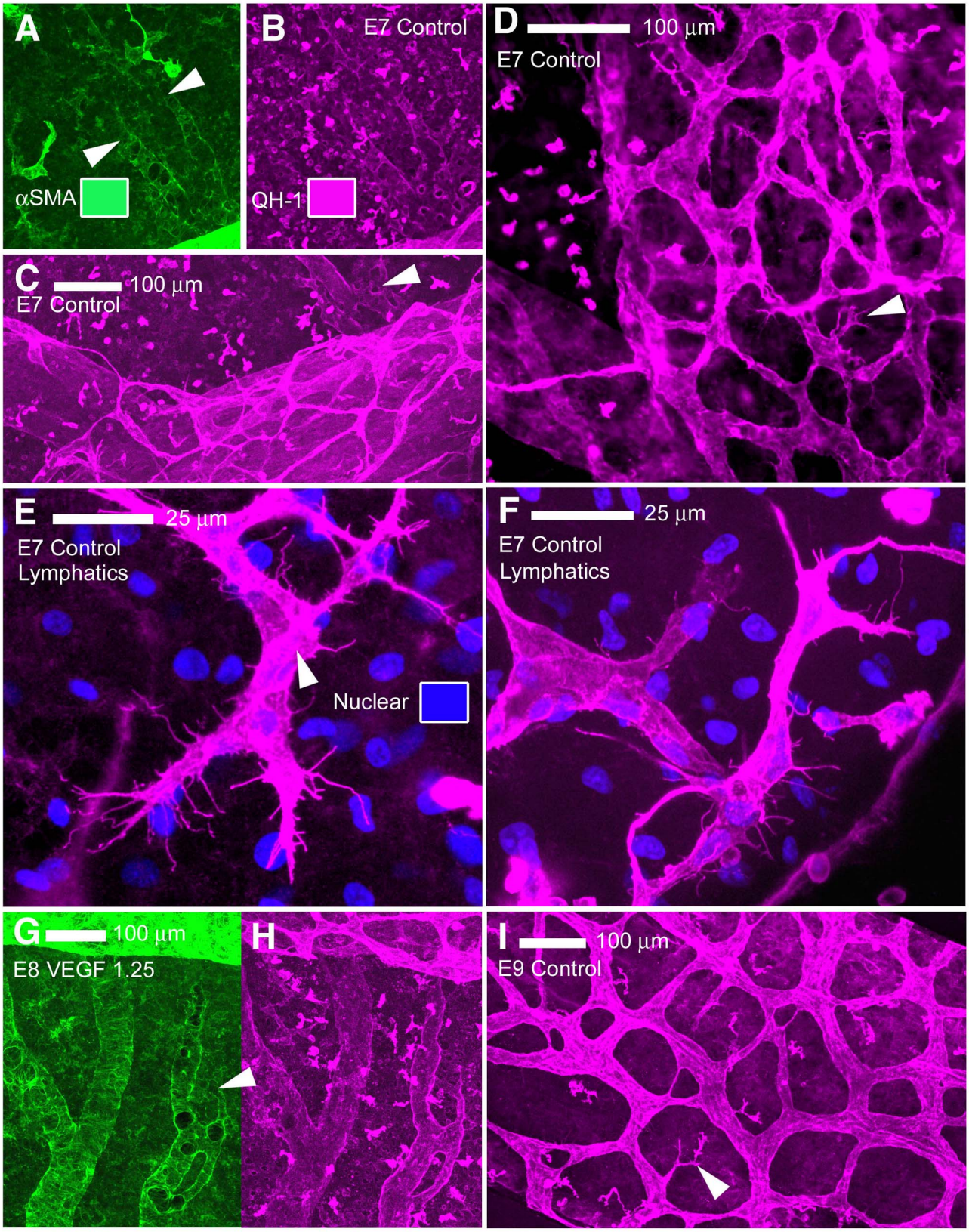

Fig. 8. Parsons-Wingerter *et al.*

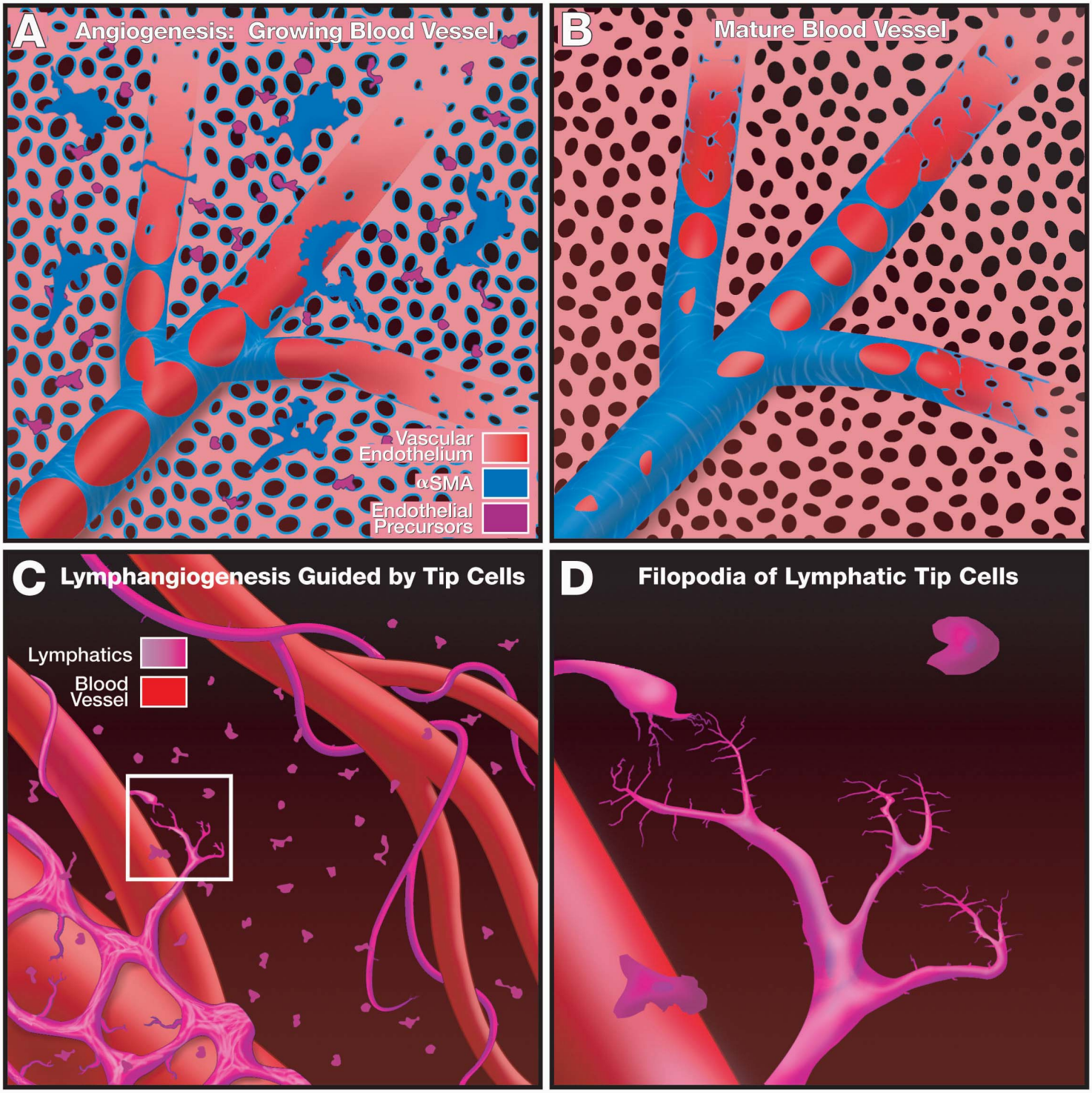

Fig. 9. Parsons-Wingerter *et al.*